Toxicology Letters 241 (2016) 71–81

Contents lists available at ScienceDirect

Toxicology Letters

journal homepage: www.elsevier.com/locate/toxlet

Impact of topical application of sulfur mustard on mice skin and distant organs DNA repair enzyme signature

Sylvie Sauvaigo[a,*], Fanny Sarrazy[a], Mohamed Batal[b,c], Sylvain Caillat[b,c], Benoit Pitiot[a], Stéphane Mouret[d], Cécile Cléry-Barraud[d], Isabelle Boudry[d], Thierry Douki[b,c]

[a] LXRepair, Grenoble, France
[b] University Grenoble Alpes, INAC, LCIB, LAN, F-38000 Grenoble, France
[c] CEA, INAC, SCIB, LAN, F-38000 Grenoble, France
[d] Institut de Recherche Biomédicale des Armées, Antenne de La Tronche, France

HIGHLIGHTS

- Topical application of sulfur mustard affects DNA repair in skin and internal organs.
- Each organ is differently affected as soon as 4 h after application of SM.
- Most glycosylase/AP endonuclease activities decrease but repair of 8oxoG increases.
- DNA excision/synthesis activities are inhibited in skin, kidneys and brain.
- Most DNA excision/synthesis activities are enhanced in lungs after SM exposure.

GRAPHICAL ABSTRACT

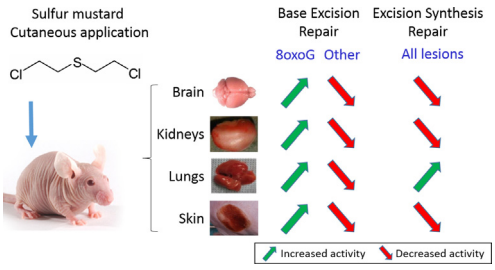

ARTICLE INFO

Article history:
Received 30 July 2015
Received in revised form 2 November 2015
Accepted 2 November 2015
Available online 10 November 2015

Keywords:
Sulfur mustard
DNA repair
DNA adducts
Oxidative stress
Inflammation
Exposure biomarker

ABSTRACT

Sulfur mustard (SM) is a chemical warfare agent that, upon topical application, damages skin and reaches internal organs through diffusion in blood. Two major toxic consequences of SM exposure are inflammation, associated with oxidative stress, and the formation of alkylated DNA bases. In the present study, we investigated the impact of exposure to SM on DNA repair, using two different functional DNA repair assays which provide information on several Base Excision Repair (BER) and Excision/Synthesis Repair (ESR) activities. BER activities were reduced in all organs as early as 4 h after exposure, with the exception of the defense systems against 8-oxo-guanine and hypoxanthine which were stimulated. Interestingly, the resulting BER intermediates could activate inflammation signals, aggravating the inflammation triggered by SM exposure and leading to increased oxidative stress. ESR activities were found to be mostly inhibited in skin, brain and kidneys. In contrast, in the lung there was a general increase in ESR activities. In summary, exposure to SM leads to a significant decrease in DNA repair in most organs, concomitant with the formation of DNA damage. These synergistic genotoxic effects are likely to participate in the high toxicity of this alkylating agent. Lungs, possibly better equipped with repair enzymes to handle exogenous exposure, are the exception.

* Corresponding author at: LXRepair; 7, Parvis Louis Néel; BP 50; 38040 Grenoble, France. Fax: +33 438785090.
E-mail address: sylvie.sauvaigo@lxrepair.com (S. Sauvaigo).

http://dx.doi.org/10.1016/j.toxlet.2015.11.001
0378-4274/

1. Introduction

Sulfur mustard (SM) is a chemical warfare agent which has been used for almost a century, first in World War I and more recently in Iraq (Balali-Mood and Hefazi, 2006) and Syria. SM is also considered as a potential chemical weapon for terrorist actions (Smith et al., 1995; Wattana and Bey, 2009). Consequently, SM remains a threat for both militaries and civilians. SM has three main targets in humans, namely eyes, lungs, and skin (Balali-Mood and Hefazi, 2005). In the latter organ, exposure to SM leads to the formation of large blisters which poorly heal (Momeni et al., 1992; Ghanei et al., 2010). SM was consequently classified as a vesicating agent. Damage to organs and in particular in skin results from a massive cell death by necrosis and apoptosis. In addition an acute inflammatory response takes place. At the molecular level, these deleterious properties are explained by the alkylating properties of SM which efficiently reacts with biomolecules.

Induction of DNA damage is proposed to be strongly involved in the lethal process (Papirmeister et al., 1985; Debiak et al., 2009; Kehe et al., 2009). Indeed, reaction of SM with DNA leads to the formation of a wide array of damage including monoadducts to guanine and adenine, inter- and intra-strand guanine biadducts (Brookes and Lawley, 1960, 1961, 1963; Fidder et al., 1994; Ludlum et al., 1994) and a recently characterized ternary glutathione-SM-guanine adduct (Batal et al., 2015). In addition exposure to SM results in GSH depletion and oxidative stress which in turn induces oxidative DNA lesions (Pal et al., 2009; Tewari-Singh et al., 2012).

Information on the *in vivo* formation of SM-DNA adducts have mostly been obtained following cutaneous exposure using either immunological detection (van der Schans et al., 2004) or HPLC-mass spectrometry quantification (Batal et al., 2013; Yue et al., 2014). Adducts were found to be readily produced, even at low doses. In addition, they are quite persistent and could be detected in skin as long as three weeks after exposure. Interestingly, even after cutaneous exposure, SM diffuses through the skin, reaches the blood and then internal organs (Cullumbine, 1946; Chilcott et al., 2000; Goswami et al., 2015; Yue et al., 2015). Among other consequences, DNA adducts are produced (Batal et al., 2014; Yue et al., 2015) with brain and lungs being the most sensitive targets.

In contrast to the formation of SM adducts, little is known about their repair. Experiments in a series of genetically deficient cells showed that nucleotide excision repair (NER), a repair mechanism handling both bulky lesions and interstrand crosslinks, was important for the repair of SM-induced DNA damage and cell survival in eukaryotes (Kircher et al., 1979; Matijasevic et al., 2001; Matijasevic and Volkert, 2007; Jowsey et al., 2012). In bacteria, evidence were also obtained for a role of both repair of interstrand crosslinks (Lawley and Brookes, 1965) and of 3-methyladenine DNA glycosylase II (Matijasevic et al., 1996). Moreover, SM-DNA adducts are unstable and can depurinate, leading to the formation of abasic sites. This class of DNA lesions is efficiently repaired in cells by AP endonucleases such APE1 (Hoeijmakers, 2001; Robertson et al., 2009). In spite of these biochemical data, no information is available on the impact of exposure to SM on the overall DNA repair efficacy and on the modulation of the different repair pathways in cells.

We designed the present study to address this latter point in order to obtain mechanistic information and propose a possible biomarker of exposure. SKH-1 hairless mice were exposed to SM on the back. DNA repair was studied in skin, brain, lungs and kidneys, the organs where the level of DNA adducts was found to be the highest in a previous study (Batal et al., 2013, 2014). DNA repair activities were quantified using two different functional DNA repair assays developed on biochips (Millau et al., 2008; Pons et al., 2010). The ODN biochip, a multiplexed version of the Oligonucleotide (ODN) Cleavage Assay, provided information on the glycosylase activities associated with the bases excision repair pathway (BER), against a series of modified bases incorporated into different ODNs. The plasmid microarray, functionalized with series of plasmids containing different small or bulky lesions, allowed us to quantify excision/synthesis repair (ESR) activities and thus was relevant to both NER and BER. These two techniques were applied to whole protein extracts from the four investigated organs and showed that SM actually modulates DNA repair activities whatever the organ investigated, through a direct impact and possibly in relation to inflammation.

2. Materials and methods

2.1. Mice exposure to SM

Male, euthymic and hairless SKH-1 mice (Crl: SKH1-hr, 4–6 weeks of age) were purchased from Charles River Laboratories (L'Arbresle, France). They were housed and acclimatized for one week before experiment with food and water *ad libitum*. Treatment was made as described elsewhere (Batal et al., 2013). All procedures were in accordance with the regulations regarding the "protection of animals use for experimental and other scientific purposes" from the relevant Directives of the European Community (86/606/CE). Study protocols were approved by the Ethical Committee of the French Armed Forces Biomedical Research Institute. Briefly, on the day of exposure, animals were anesthetized (ketamine hydrochloride and diazepam) and randomly assigned to treatment groups ($n = 3$). For pain relief, buprenorphin (0.05 mg/kg) was delivered by a subcutaneous injection. SM, diluted in 2 μL of dichloromethane, was topically applied on an ink-marked circular zone of 0.28 cm^2 on the dorsal–lumbar region of the animal (Dorandeu et al., 2011). Animals were exposed to SM dose of either 0.6 or 6 mg/kg. SM was removed from the skin after 4 h using 0.8% sodium hypochlorite and natural sponges. Four hours or 24 h after the end of the exposure, mice were euthanized by intraperitoneal injection of a lethal dose of pentobarbital (100 mg/kg). Brain, lungs, kidneys and skin punches (8 mm diameter at the treated site) were rapidly collected and processed immediately for extract preparation. The mice identification numbers and the corresponding treatment conditions are listed in Table S1.

2.2. Preparation of whole cell extracts from mice organs

The fresh organs were cut into small slices, and placed in 2 mL of ice-cold HEPES/KOH 90 mM pH 7.8, KCl 0.8 M, EDTA 2 mM, glycerol 20%, DTT 1 mM. They were then disrupted and homogenized for 30 s at medium speed using the Qiagen TissueRuptor®. The lysis was completed by one cycle of freezing/thawing in liquid nitrogen and 4 °C, respectively. A second ice-cold buffer (150 μL) was subsequently added (HEPES/KOH 45 mM pH 7.8, EDTA 0.25 mM, glycerol 2%, 5 mM phenylmethane sulfonyl fluoride) before a second round of freezing/thawing. Lastly the lysates were cleared by 5 min centrifugation at 16 000 g at 4 °C and stored frozen in 100 μL aliquots at −80 °C. The protein concentration was determined in each sample using the BCA kit (Interchim, Montluçon, France).

2.3. DNA repair assays

2.3.1. Multiplexed ODN cleavage assay

A panel of DNA duplexes, each containing a different lesion repaired by BER, were immobilized at specific sites on glass slides, forming 24 identical pads. On each pad, a control ODN (Lesion_Free ODN) and eight lesion-containing ODNs were available in

duplicate: 7,8-dihydro-8-oxo-guanine (8oxoG) paired with C (8oxoG-C), adenine (A) paired with 8oxoG (A-8oxoG), thymine glycols (Tg) paired with A (Tg-A), tetrahydrofuran (THF), as an AP site substrate equivalent, paired with A (THF-A), hypoxanthine (Hx) paired with thymine (T) T (Hx-T), ethenoadenine (EthA) paired with T (EthA-T), and uracil (U) in front of either G (U-G) or A (U-A). The lesions containing-ODNs were labeled at their end by a Cy3. Cleavage of the lesions by the enzymes contained in the extracts led to the release of the corresponding fluorescence. Each slide comprised two wells incubated by the excision buffer only which served as reference (100% fluorescence) to calculate the lesions percentage of excision for the wells incubated with the extracts. A supplementary normalization was performed that took into account the possible degradation of the Lesion_Free ODN in each well. The percentage of excision of each lesion was then calculated using the following formula: (100 × (1-percentage of fluorescence of Lesion_ODN/percentage of fluorescence of Lesion_-Free ODN)).

The excision reactions were conducted using a protein concentration of 10 μg/mL at 30 °C for 60 min in 80 μL of excision buffer (10 mM Hepes/KOH pH 7.8, 80 mM KCl, 1 mM EGTA, 0.1 mM $ZnCl_2$, 1 mM DTT, 0.5 mg/mL BSA). The slides were subsequently rinsed at room temperature (RT) 3 × 5 min with 80 μL of washing buffer (PBS containing 0.2 M NaCl and 0.1% Tween 20) and dried for 5 min at 37 °C. The fluorescence quantification was performed using the Innoscan scanner from Innopsys (Toulouse, France). Each extract was tested twice. The results between the replicates (4 spots) were normalized using the NormalizeIt software as described in Millau et al. (2008).

2.3.2. Multiplexed excision/synthesis repair (ESR) assay

The multiplexed ESR assay on support has already been described in detail in Millau et al. (2008). Briefly, it is based on the immobilization on a hydrogel coated glass slide of a series of supercoiled double-stranded plasmid DNA which bear specific DNA lesions. Several modifications are available: photoproducts (a mixture of cyclobutane pyrimidine dimers (CPD) and (6–4) photoproducts (64)), 8oxoGua, alkylated bases (AlkB), abasic sites (AbaS), glycols (thymine and cytosine glycols), cisplatin (CisP) and psoralen (Pso) adducts. The repair reactions are conducted in the presence of the cell extract of interest and of dCTP-Cy3, and result in the incorporation of fluorescence at the damaged plasmid sites upon repair. ESR reactions were conducted using a protein concentration of 0.4 mg/mL at 30 °C for 2 h. The slides were subsequently rinsed 3 × 5 min in water. Each extract was tested twice. The total fluorescence intensity of each spot was quantified using the Innoscan scanner from Innopsys (Toulouse, France).

2.4. Data analysis

2.4.1. Multiplexed ODN cleavage assay

For each exposure time and each SM concentration, for each lesion, the mean of the excision percentage of the 3 control samples (Non Treated mice) was calculated. This mean was subtracted to each value (excision percentage) obtained for the treated mice. Then, for each lesion, the data were normalized (centered around 0 with a standard deviation of 1).

2.4.2. Multiplexed excision/synthesis repair assay

Data (Fluorescence Intensity (FI)) were log10-transformed. For each exposure time and each SM concentration, we calculated the mean of the FI of the 3 control samples (Non Treated mice) for each lesion. This latter value was subtracted to the value corresponding to the ESR of each lesion.

2.4.3. Hierarchical clustering

We then performed unsupervised hierarchical clustering using the Euclidean dissimilarity measure and average linkage agglomeration method, to group the samples by similarities across the organs response, according to exposure time and SM concentration.

To assess uncertainty in hierarchical cluster analysis the *p*-values (AU (Approximately Unbiased) *p*-value) were calculated *via* multiscale bootstrap resampling using the pvclust R package (available at https://cran.r-project.org/). The *p*-values on the dendrograms are transformed in 100 × (1-*p*-value).

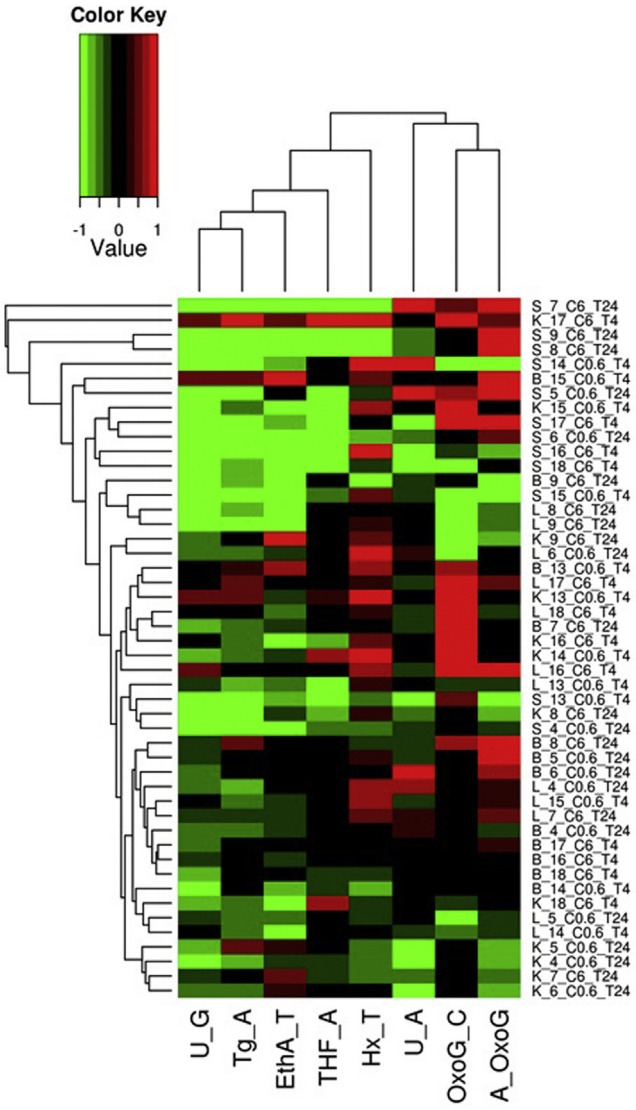

Fig. 1. Heat-Map representation of the variation in BER activities across the organs (skin (S), lungs (L), brain (B) and kidney (K)) and treatment conditions (C0.6 and C6 for exposure dose of 0.6 and 6 mg/kg, respectively, and T4 and T24 for exposure time of 4 h and 24 h, respectively). Three mice were used for each treatment condition. Each sample was identified by the organ type (S, L, B or K) followed by the animal identity number (see Table S1), the compound concentration (C06 or C6) and the exposure time (T4 or T24). Values greater than 0 are represented in red. They reflect an induction of the repair activity by SM. Values below 0 are represented in green. They indicate an inhibition of the repair activity by SM. Values around 0 are represented in black indicating no effect of SM. (For interpretation of the references to colour in this figure legend, the reader is referred to the web version of this article.)

2.4.4. Statistical test

To examine the significant induction or inhibition of the different repair activities by SM we used the non-parametric Wilcoxon test for the groups containing >4 samples. When sample number within a group was ≤4, induction or inhibition was considered significant when |mean| > 3 × standard error.

3. Results

3.1. Base excision repair

3.1.1. Basal level

Using ODN biochip, we first compared the level of glycosylase activity in the different organs of control mice (Fig. S1). Large differences were observed for the repair of most lesions. The most efficient cleavage rate, whatever the organ considered, concerned THF, the abasic site analog, which is cleaved by the endonuclease APE1 (cleavage rates comprised between 55% and 90%). Excision rates of 8oxoG-C, A-8oxoG and U-A were particularly low in all organs (generally <10%). The cleavage rates for the other lesions ranged between 15 and 30% (EthA-T, Hx-T, U-G, Tg-A).

3.1.2. Dose effect

Measurements were made in mice exposed to increasing dose of SM on dorsal skin. Quantification was performed in skin and in internal organs. Following appropriate normalization and averaging within the different groups of mice, dose-dependent modulations of some repair activities were observed (Fig. S1). Variations were shown at both 4 h and 24 h but not always with the same trend at both times depending on the lesion.

3.1.3. Classification of the BER profiles obtained for the different organs and the different treatment conditions

Extensive analysis of the data was performed with all animals considered individually. First, a heat map was drawn (Fig. 1). The dendrogram classification showed that profiles were mainly classified according to organ type and exposure time (Fig. 2). First, this observation reflects that each organ exhibits a distinct BER capacity profile. Second, as the two exposure concentrations ($C = 0.6$ and $C = 6$ mg/kg) were usually mixed within the same classes, it can be concluded that the SM concentration was less important than exposure time and organ to discriminate the samples for the classification. We focused only on the main

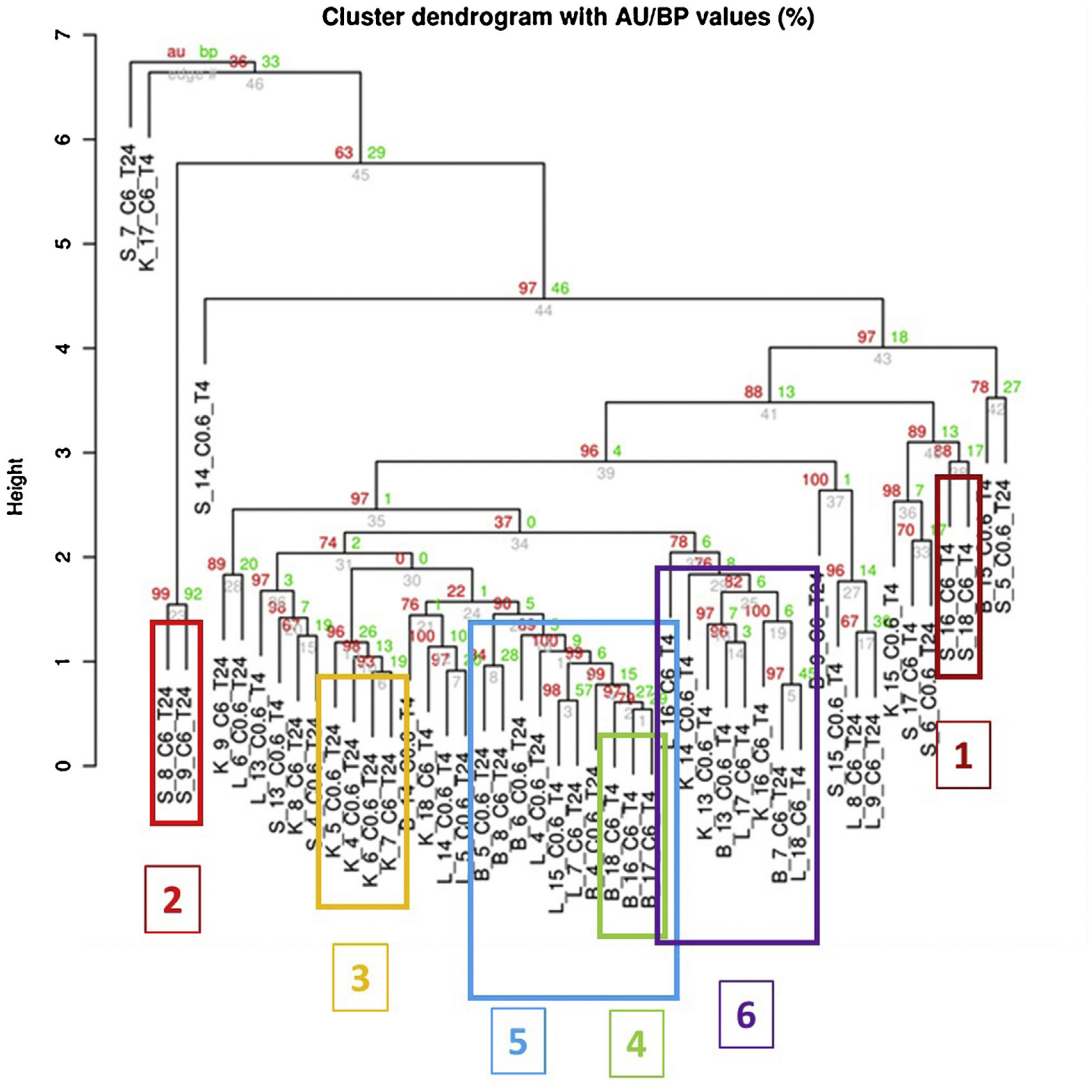

Fig. 2. Dendrogram created from the hierarchical clustering of the BER activities profile variation obtained from the Skin (S), Brain (B), Kidney (K) and Lungs (L) samples coming from mice treated with 2 concentrations of SM (C0.6 = 0.6 mg/kg and C6 = 6 mg/kg) and analyzed at 2 time points (T4 = 4 h and T24 = 24 h). Three mice were used for each treatment condition (See Table S1).

Table 1
Characteristics of the clusters.

Group number	Group name	Characteristics	Group size	AU *p*-value
1	S_T4	S T4 C6 (2)	2	88
2	S_T24	S T24 C6 (2)	2	99
3	K_T24	K T24 C0.6 (3), K T24 C6 (1)	4	96
4 (sub-group of 5)	B_T4	B T4 C6 (3)	3	97
5	B_T4 BL_T24	B T4 C6 (3), B T24 C0.6 (3), B T24 C6 (1), L T4 C0.6 (1), L T24 C0.6 (1), L T24 C6 (1)	10	90
6	KL_T4	K T4 C0.6 (2) K T4 C6 (1) L T4 C6 (3)	6	78

Organs: B—Brain, K—Kidney, L—Lung, S—Skin; Exposure time: T4 = 4 h, T24 = 24 h; SM concentration: C0.6 = 0.6 mg/kg, C6 = 6 mg/kg; Into brackets: number of individuals (mice). The AU *p*-value characterizes the significance of the main classes obtained.

identified clusters described in Table 1: six groups were identified. Statistical analysis was performed to assess the significance of the modulation of DNA repair for these groups. The complete results are reported as supplementary information (Table S2) and summarized in Table 1 and Fig. 3. They show that the range of variation in BER activity as a response to SM greatly differs from one organ to the other. The most sensitive one is skin, which is expected as it is the treatment site. Then lungs and kidneys are similarly affected at 4 h. At 24 h similar effects are observed for brain and lungs. As can be seen in Fig. 4, repair of U-G, Tg-A, EthA-T and THF-A lesions was mostly down regulated. In contrast, that of Hx-T and 8oxoG-C was improved in kidney and lung at 4 h. Similarly repair of A-8oxoG was stimulated in skin, brain and lung at 24 h.

Organs: B—Brain, K—Kidney, L—Lung, S—Skin; Exposure time: T4 = 4 h, T24 = 24 h ; SM concentration: C0.6 = 0.6 mg/kg, C6 = 6 mg/kg; Into brackets: number of individuals (mice). The AU *p*-value characterizes the significance of the main classes obtained.

3.2. Excision/synthesis repair

3.2.1. Basal level

As observed for BER activities, large differences were observed for ESR between the organs. ESR activities were found to be quite low in skin. They were larger in lungs and kidneys, with similar levels in the two organs. Brain exhibited the highest ESR activity among investigated organs (Fig. S2).

3.2.2. Dose effect

Quantification of ESR activities against a series of DNA lesions located within plasmids showed that SM modulated these repair pathways like it did for the excision step of BER. Compared to basal level, SM application resulted in decrease of ESR activities in skin, brain and kidneys while an increase was observed in lungs at 4 h for certain SM concentrations (Fig. S2).

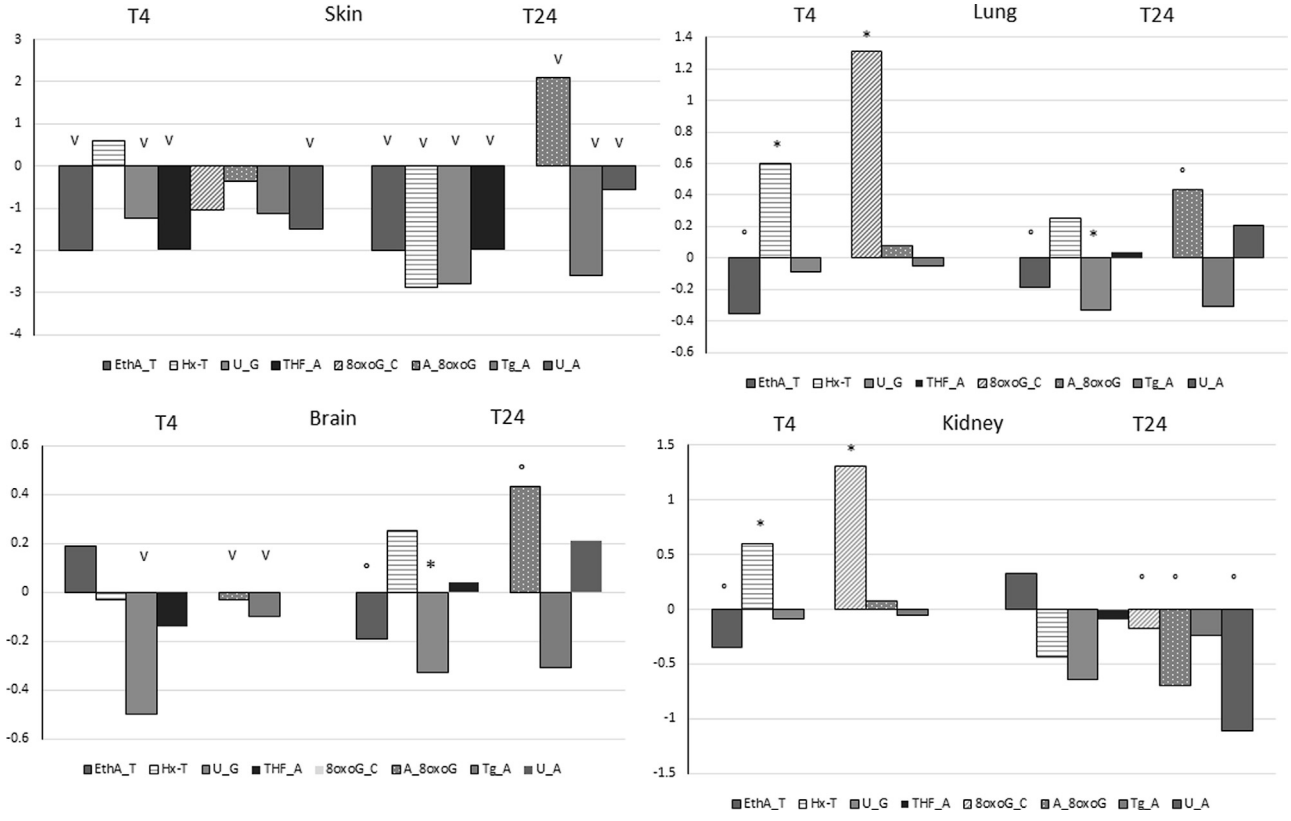

Fig. 3. Quantitative variation of the BER activities obtained for the two exposure times: the vertical axis shows the difference between control and treated mice at 4 h and 24 h for each lesion. Significant results are labeled by *($p < 0.05$), °($p < 0.1$) (Wilcoxon test) or by v when |mean| > 3 × standard error for the classes containing a small number of individuals (≤4).

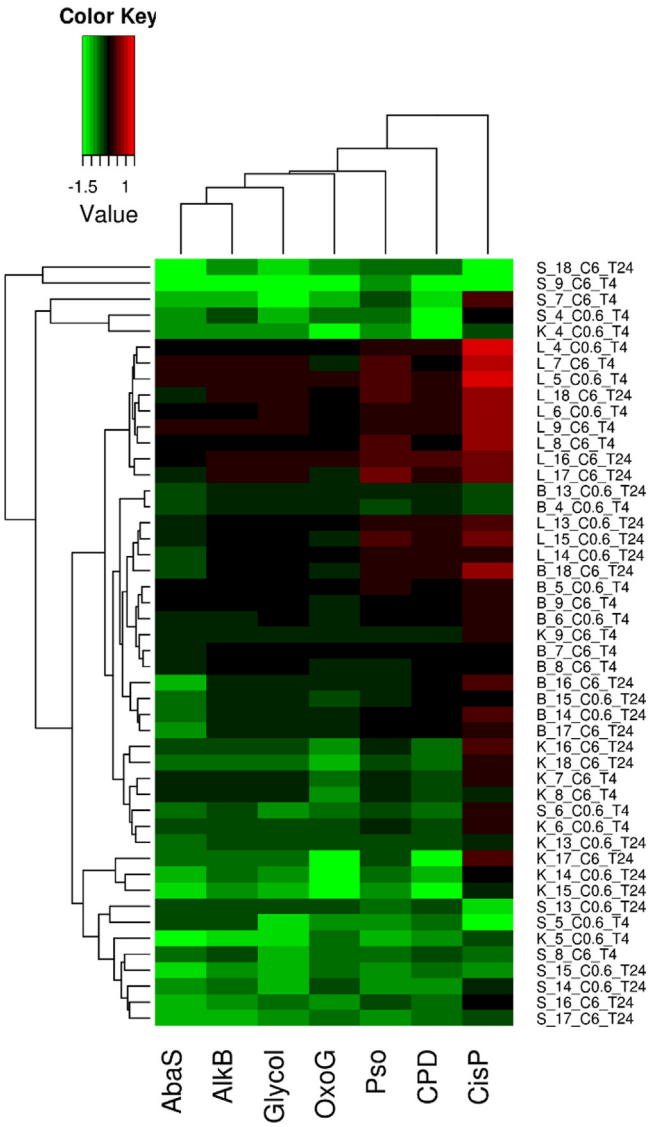

Fig. 4. Heat-Map representation of the ESR activities variation across the organs and treatment conditions. The mice were treated using 2 different doses of SM (0.6 and 6 mg/kg (C0.6 and C6, respectively)), and 2 exposure times (4 h and 24 h (T4 and T24, respectively)). Each sample was identified by the organ type (S (skin), L (lung), B (brain) or K (kidney)) followed by the animal identity number (See Table S1), the compound concentration (C0.6 or C6) and the exposure time (T4 or T24). Three mice were used for each treatment condition. Values greater than 0 are represented in red. They reflect an induction of the repair activity by SM. Values below 0 are represented in green. They indicate an inhibition of the repair activity by SM. Values around 0 are represented in black indicating no effect of SM. (For interpretation of the references to colour in this figure legend, the reader is referred to the web version of this article.)

3.2.3. Classification of the ESR profiles obtained for the different organs and the different treatment conditions

The heat map drawn with all individual data (Fig. 4) shows that results are essentially classified by organ type. This reflects the fact that the different organs displayed distinguishable DNA Repair Enzyme Signature in response to SM exposure. The color code revealed the trend to increasing ESR in lungs (red color) while decrease is observed other organs. As can be seen from the dendrogram (Fig. 5), seven different significant clusters (Group G1–G7) were identified. They are described in Table 2 together with the class significance. The seven groups listed in Table 3 were also clustered in larger significant groups demonstrating that, despite their differences, they share important similarities (G2–G5; AU p-value = 99), (G2–G3–G5–G6; AU p-value = 96), (G1–G2–G3–G5–G6; AU p-value = 99), (G4–G7; AU p-value = 99). This separation according to organ type allowed to gain information on the response specificity of each organ. The statistical analysis permitted the determination of the significant impact (induction/inhibition) of SM on the different ESR activities and revealed the differences between organs (Table S3 and Fig. 6).

3.2.4. Correlation between ESR activity and level of DNA adducts

The latter results unambiguously showed that SM actively modulated the ESR activity in some organs at different times. We thus studied whether these variations could be correlated to the level of DNA adduct determined in our previous works (Batal et al., 2013, 2014). At 4 h, a negative correlation reaching significance in half of the cases was found (Table 3). It illustrates in a different way the trend to a negative impact of SM on DNA repair. At 24 h, the trend is less obvious because of the decrease in the level of DNA adducts, the rate of which is different from one organ to the other. Consequently, the level of DNA damage is less related to the initial dose of SM reaching the organ. Yet, some significant negative correlations are still observed for repair of cisplatin adducts and psoralen adducts.

4. Discussion

SM is a chemical warfare agent known to damage tissues partly through the induction of massive DNA damage. Information are available on the formation of SM adducts to DNA both *in vitro* and *in vivo* but very little is known about their repair. We thus undertook this work to determine whether cutaneous exposure of mice affected repair in skin as well as in internal organs where SM diffuses through blood. For the measurement of DNA repair activities, we used parallelized micro-arrays in order to simultaneously gather information on the repair of several specific lesions. Both the excision step of BER and ESR were investigated. It should first be stressed that, even in the absence of exposure, drastic differences could be determined for the basal level of repair between the different organ. For instance, ESR activity in skin was found to be 10% of that in brain. To the best of our knowledge, it is the first time that such differences have been reported. As far as BER is concerned, a largely predominant activity of APE1 was observed in the extracts. This result is consistent with our previous observations made with human fibroblasts extracts (Pons et al., 2010), with HeLa cells extracts (Candeias et al., 2010), with *Drosophila* mitochondria extracts (Garreau-Balandier et al., 2014) and with data from the literature (Cappelli et al., 2001; Visnes et al., 2008). Interestingly, the other BER activities that were detected in the different mice tissues were rather low compared to what is generally observed with cultured human cell extracts.

The exposure scheme we followed in the present animal study was similar to that applied to the study of the formation of DNA adducts (Batal et al., 2013). An early time was chosen, corresponding to an almost asymptomatic phase at the doses used, followed by a time point at 24 h where inflammation and formation of an edema at the treated site take place. Differences between organs were observed in terms of response of DNA repair to these SM treatments. Yet effects on BER and on ESR were observed in all of them even for the lowest dose and at the earliest time. This illustrates the ability of SM not only to damage the exposed site but also to reach distant organs (Cullumbine, 1946; Chilcott et al., 2000) and trigger a DNA damage response that affects multiple DNA repair pathways. An additional mechanism could be a long-distance effect of the strong oxidative stress induced in skin by exposure to SM. Indeed, it was reported that DNA damage can be induced as a "bystander effect" of the presence of tumor cells and the associated oxidative stress (Martin et al., 2011; Glebova et al.,

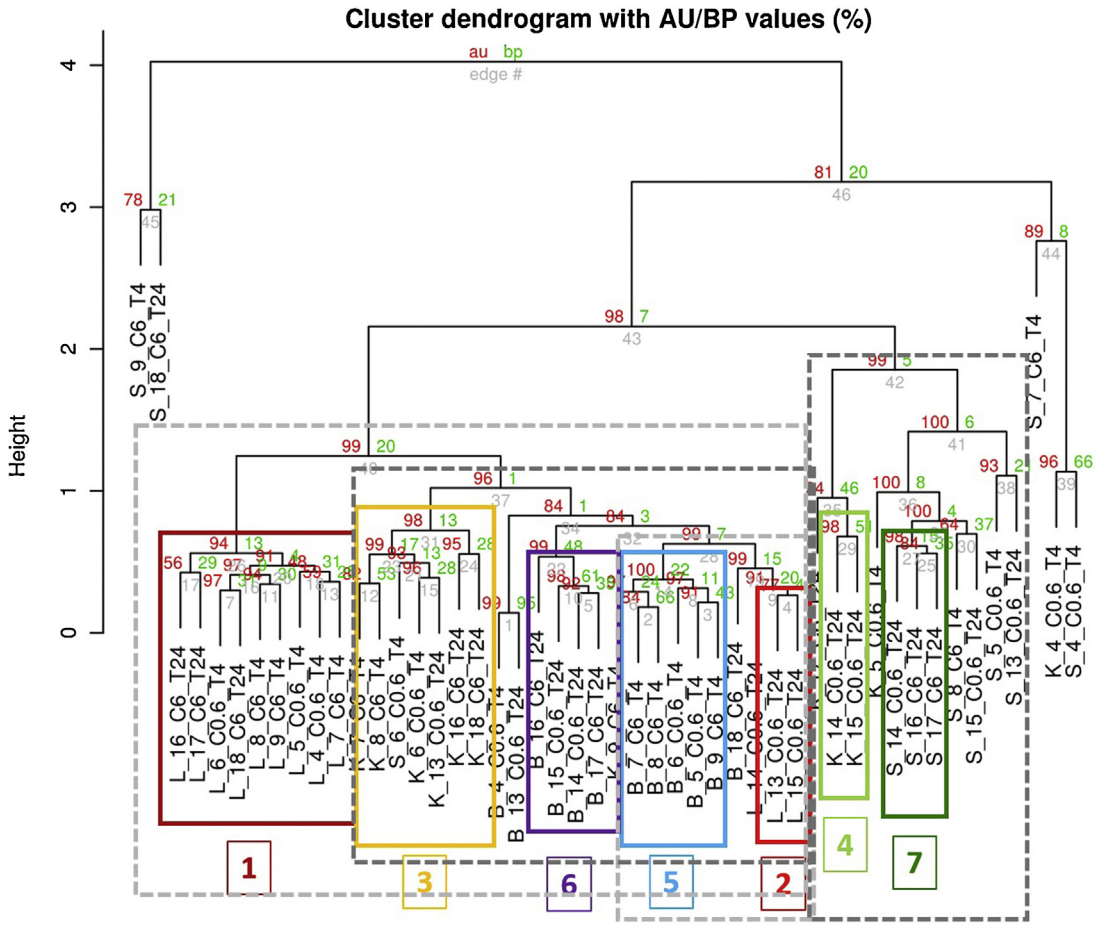

Fig. 5. Dendrogram of the ESR activities in organs of mice cutaneously exposed to either 0.6 (C0.6) or 6 (C6) mg/kg of SM for 4 h (T4) and 24 h (T24). Three mice were used for each treatment condition. Each sample was identified by the organ type (S (skin), L (lung), B (brain) or K (kidney)), followed by the animal identity number (See Table S1), the compound concentration (C0.6 or C6) and the exposure time (T4 or T24).

Table 2
Characteristics of the different identified clusters determined for the ESR activities.

Group number	Group name	Characteristics	Group size	AU *p*-value
G1	L_1	L C0.6 T4 (3), L C6 T4 (3), L C6T24 (3)	9	94
G2	L_C0.6_T24	L C0.6 T24 (3)	3	91
G3	K_1	K C6 T4 (2), K C0.6 T4 (1), K C0.6 T24 (1), K C6 T24 (2)	6	98
G4	K_C0.6_T24	K C6 T24 (2)	2	98
G5	B_T4	B C6 T4 (3), B C0.6 T4 (2)	5	100
G6	B_T24	B C6 T24 (2), B C0.6 T24 (2)	4	99
G7	S_T24	S C0.6 T24 (1), B C6 T24 (2)	3	98

Organs: B—Brain, K—Kidney, L—Lung, S—Skin; Exposure time: T4 = 4 h, T24 = 24 h; SM concentration: C0.6 = 0.6 mg/kg, C6 = 6 mg/kg.

2015). We have clearly previously observed *in vitro* a link between ROS production and decreased repair capacities measured by our biochips. A first example is the effect oxidative stress in a cellular model of Alzheimer disease (Forestier et al., 2012). Conversely, improved BER has been observed as an effect of selenium which exhibits antioxidant properties (de Rosa et al., 2012).

In the case of BER, modulation of excision activities was found to differ from one organ to the other. Yet, similarities in repair profile were observed between kidney and lungs at 4 h and between brain and lungs at 24 h. Skin, being directly exposed to SM, is the organ where modulation was the most intense. In contrast, little modification of BER excision activity was observed in brain although SM efficiently reaches it as shown by the fact that it is the internal organ exhibiting the largest amounts of DNA adducts after topical exposure. It may be proposed that brain, being

Table 3
Correlation coefficient[a] between the level of SM DNA adducts[b] and the excision/synthesis repair efficiency for three DNA lesions repaired by NER, as SM-adducts (CPD: UV-induced pyrimidine dimers, CisP: Cisplatin DNA adducts, Pso: UVA-induced DNA adduct between DNA and psoralen). Data from lung, brain, kidney and skin were combined. High frequency of SM DNA adducts (HETE-N7G, N7G-ETE-N7G, HETE-N3A) was inversely correlated with ESR efficiency, especially at 4 h.

Treatment time	4 h			24 h		
Adducts\repair	CPD	CisP	Pso	CPD	CisP	Pso
HETE-N7G	−0.80	−0.98*	−0.94°	−0.55	−0.96*	−0.91°
N7G-ETE-N7G	−0.83	−0.98*	−0.94°	−0.30	−0.92°	−0.79
HETE-N3A	−0.65	−0.95°	−0.87	0.65	0.31	0.45

[a] Statistical significance: $^{*}p < 0.05$ and $^{\circ}p < 0.1$.
[b] Data were taken from (Batal et al., 2013, 2014).

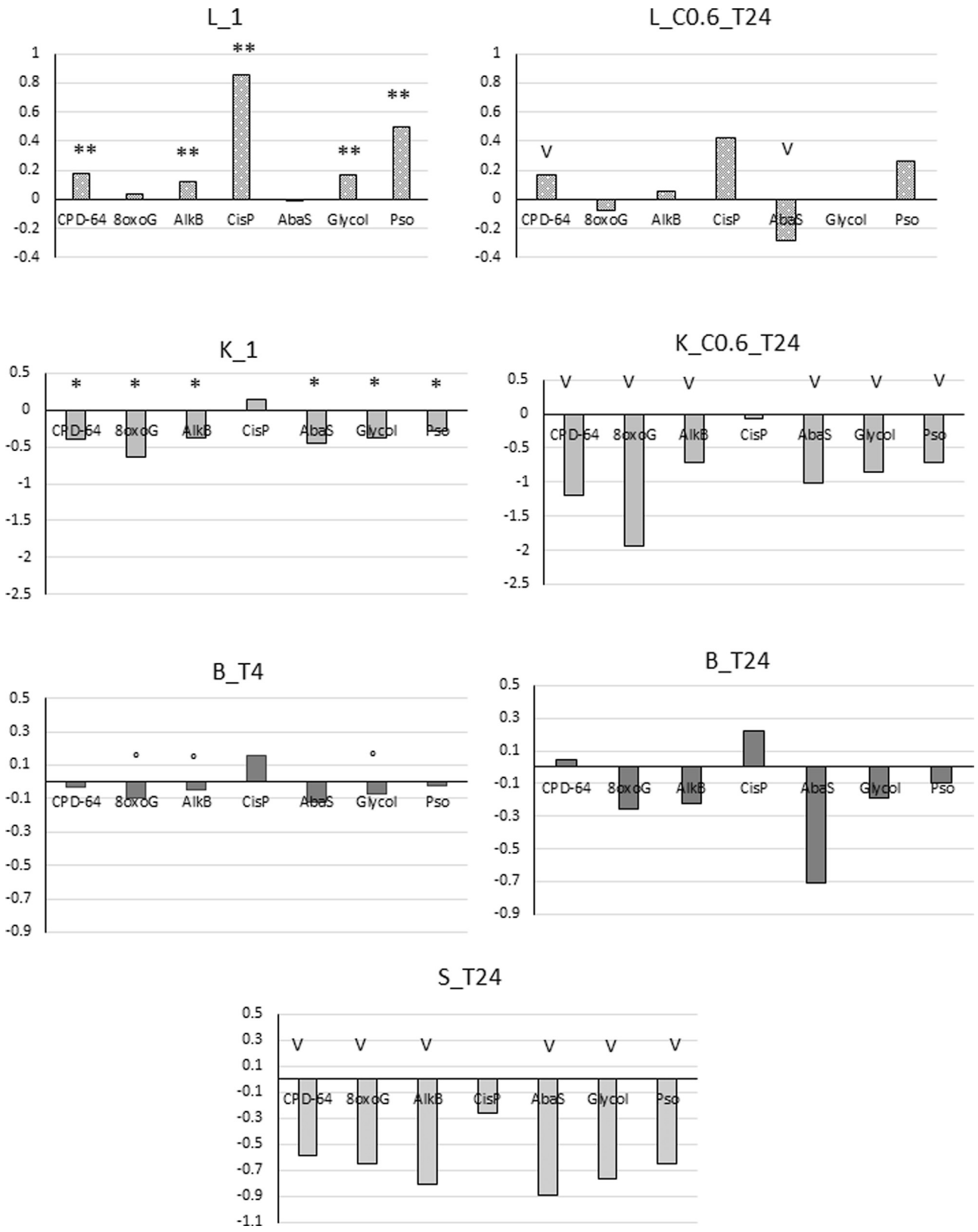

Fig. 6. Quantitative variation of the ESR activities by organ and according to significant group (normalized data) Significant results are labeled by *($p < 0.05$), °($p < 0.1$) (Wilcoxon test) or by v when |mean| > 3 × standard error for the classes containing a small number of individuals (≤4).

subject to high level of oxidative stress as the result of a large energy consumption, already exhibits large BER activities in the absence of exposure.

Among the modulated BER activities, a few were found to be upregulated. The first is hypoxanthine repair that was found to be induced at 4 h in lungs and at 24 h in kidneys. In mice hypoxanthine

repair is initiated by the AAG (Alkyladenine DNA Glycosylase) known also as MPG (*N*-Methyl Purine DNA Glycosylase) (Engelward et al., 1997). This enzyme is in charge of removing a wide variety of alkylated, deaminated and lipid-peroxidation-induced purine adducts from the genome. In particular its substrates include, in addition to hypoxanthine, 3-methyladenine, 7-methylguanine and 1,N^6-ethenoadenine (Smith and Engelward, 2000). Interestingly, SM is a powerful alkylating agent leading to the formation of adducts mainly at positions 3 and 7 of adenine and guanine bases, respectively (Brookes and Lawley, 1960, 1961, 1963; Fidder et al., 1994; Ludlum et al., 1994). Consequently it is logical to hypothesize that AAG is specifically induced in lung and kidney to counteract the genotoxic effects induced by the topical application of SM.

Another induced DNA repair machinery is that which processes 8-oxoG lesions. At 4 h, two organs displayed enhanced cleavage of 8oxoG (Kidneys and Lungs). The oxidized base 8oxoG is a major mutagenic purine derivative. It is primarily removed from 8oxoG:C pairs by OGG1. When 8oxoG escapes this repair and subsequent replications occur, the polymerases incorporate an A across of 8oxoG leading to an A:8oxoG mispair. In mammalian cells, MYH cleaves A from A:8oxoG mispairs and recruits an AP endonuclease to cleave the residual AP site (Luncsford et al., 2013). Hence, MYH serves as back-up system for the removal of the 8oxoG. Strikingly, 3 organs displayed enhanced cleavage of A paired with 8oxoG 24 h after exposure to SM. Considering the temporal relationship between MYH activity and 8oxoG replication, it is not surprising that the up-regulation occurs 24 h after exposure to SM. Induction of OGG1 activity and subsequently of MYH activity could be related oxidative stress. As a matter of fact, SM exposure is known to induce oxidative stress first directly through the consumption of glutathione by alkylation (Papirmeister et al., 1985; Tewari-Singh et al., 2012) and second, more systemically, as the result of induction of inflammation (Kehe et al., 2009).

We previously reported strong evidence of the induction of a fast acute inflammation reaction in the SKH-1 mice exposed to SM (Mouret et al., 2015). This response may explain induction of the 3 above-mentioned repair enzymes. Indeed BER is known to repair lesions created by reactive oxygen and nitrogen species (RONS) released during the inflammation process. This concerns in particular oxidized, deaminated and ethenobases (Calvo et al., 2012) that are eliminated through the activity of OGG1, MYH and AAG. Importantly, recent publications mention the pro-inflammatory role of OGG1-initiated BER (Ba et al., 2014b; Aguilera-Aguirre et al., 2015). The OGG1/8-oxoG complex could activate small GTPase(s) signals leading to the expression of pro-inflammatory genes, maintaining a chronic inflammation (Ba et al., 2014a). Similarly, a recent paper from the Samson's group demonstrated that AAG-initiated BER generates abasic sites that in turn transforms into DNA strand breaks (Ebrahimkhani et al., 2014). These BER intermediates have been shown to activate sterile inflammation response, thereby increasing formation of ROS and RNS and the oxidative stress to DNA leading to increased expression OGG1 and AAG in the different mice organs. Activation of the latter enzyme could also result from the formation of alkylated bases and participate in the aggravation of the inflammation process.

The trend to a decrease in excision activities of BER was also observed for excision/synthesis of BER and NER in brain, skin and kidneys. Inhibition was particularly drastic in the latter organ, both at 4 h and 24 h. A strong effect was also observed in brain, in particular at 24 h. The ESR activities in skin were all very low at basal state but still decreased upon exposure to SM. Strikingly, it is interesting to note that BER-triggered single strand breaks, as a consequence notably of AAG action, induce Parp 1 hyperactivation leading to depletion in NAD+/ATP pool (Ebrahimkhani et al., 2014). We hypothesize that ATP depletion, in turn, might compromise critical enzyme functions (helicases, polymerases) related to excision/synthesis mechanisms (Araujo et al., 2000; Oksenych et al., 2009), explaining the inhibition of most ESR in skin, brain, and kidney. It should also be noted that Parp-mediated depletion of ATP as a result of formation of adducts to DNA is a proposed mechanism for the toxicity of SM (Papirmeister et al., 1985).

Lungs were the only organ in which ESR was enhanced under all conditions. In particular, repair was increased for bulky adducts and alkylated bases which are known to be handled by nucleotide excision repair like SM DNA adducts. Altogether, the lungs are the only organs where the expected increase in ESR in response to a genotoxic stress was observed. This may reflect the fact that lungs are constantly exposed to xenobiotics through inhalation and that pulmonary cells possibly have to handle a larger load of DNA damage than other cells.

In spite of this activation in lungs, a decrease in ESR capacities was observed in the other organs studied. We wanted to address the question of the dose effect. This point is relatively easy to study in skin which is the direct target of the topical treatment. In contrast no straightforward prediction can be done for the amount of SM reaching internal organs because it depends on vascularization, fat content and other parameters as reported for instance for BaP (Marie et al., 2010; Liu et al., 2014). We thus decided to use the level of DNA adducts, determined in our previous works, as a surrogate for the dose of SM in the different organs. Among DNA repair activities, emphasis was placed on three lesions handled by NER because this pathway repairs SM DNA adducts. A high inverse correlation was found at the earliest time between the frequency of DNA adducts and DNA repair efficacy. This further emphasizes the impact of SM on mechanisms involved in the maintenance of DNA integrity.

5. Conclusion

In summary, we showed here that, in response to the alkylating and pro-inflammatory compound SM applied topically, rapid and elaborate modifications are observed at the level of major DNA repair activities, following systemic diffusion of the compound to distant organs. The use of our parallelized DNA repair assays on microarrays allowed for the first time a precise characterization of the various activities in an *in vivo* study, emphasizing the complexity of the DNA damage response. The observed variations in DNA repair are organ-specific and follow a complex regulation involving inhibition and stimulation of specific DNA repair activities. The synergistic combination of the formation of high levels of various adducts and inhibition of critical DNA repair activities likely explains the high toxicity of this agent. Concomitant inflammation could worsen the cancer risk associated with exposure to strong alkylating agents such as SM. The use of the DNA repair microarrays could help identify biomarkers of risk as a consequence to SM exposure.

Conflict of interest

None.

Acknowledgements

This work was supported by the French "Agence Nationale pour la Recherche" (ToxYp project, #ANR-10-CSOSG-002-02) and the Direction Générale de l'Armement (Defense Ministry).

Appendix A. Supplementary data

Supplementary data associated with this article can be found, in the online version, at http://dx.doi.org/10.1016/j.toxlet.2015.11.001.

References

Aguilera-Aguirre, L., Hosoki, K., Bacsi, A., Radak, Z., Wood, T.G., Widen, S.G., Sur, S., Ameredes, B.T., Saavedra-Molina, A., Brasier, A.R., Ba, X., Boldogh, I., 2015. Whole transcriptome analysis reveals an 8-oxoguanine DNA glycosylase-1-driven DNA repair-dependent gene expression linked to essential biological processes. Free Radic. Biol. Med. 81, 107–118.

Araujo, S.J., Tirode, F., Coin, F., Pospiech, H., Syvaoja, J.E., Stucki, M., Hubscher, U., Egly, J.M., Wood, R.D., 2000. Nucleotide excision repair of DNA with recombinant human proteins: definition of the minimal set of factors, active forms of TFIIH, and modulation by CAK. Genes Dev. 14, 349–359.

Ba, X., Aguilera-Aguirre, L., Rashid, Q.T., Bacsi, A., Radak, Z., Sur, S., Hosoki, K., Hegde, M.L., Boldogh, I., 2014a. The role of 8-oxoguanine DNA glycosylase-1 in inflammation. Int. J. Mol. Med. 15, 16975–16997.

Ba, X., Bacsi, A., Luo, J., Aguilera-Aguirre, L., Zeng, X., Radak, Z., Brasier, A.R., Boldogh, I., 2014b. 8-oxoguanine DNA glycosylase-1 augments proinflammatory gene expression by facilitating the recruitment of site-specific transcription factors. J. Immunol. 192, 2384–2394.

Balali-Mood, M., Hefazi, M., 2005. The pharmacology, toxicology, and medical treatment of sulphur mustard poisoning. Fundam. Clin. Pharmacol. 19, 297–315.

Balali-Mood, M., Hefazi, M., 2006. Comparison of early and late toxic effects of sulfur mustard in Iranian veterans. Basic Clin. Pharmacol. Toxicol. 99, 273–282.

Batal, M., Boudry, I., Mouret, S., Clery-Barraud, C., Wartelle, J., Berard, I., Douki, T., 2014. DNA damage in internal organs after cutaneous exposure to sulphur mustard. Toxicol. Appl. Pharmacol. 278, 39–44.

Batal, M., Boudry, I., Mouret, S., Wartelle, J., Emorine, S., Bertoni, M., Bérard, I., Cléry-Barraud, C., Douki, T., 2013. Temporal and spatial features of the formation of DNA adducts in sulphur mustard-exposed skin. Toxicol. Appl. Pharmacol. 273, 644–650.

Batal, M., Rebelo-Moreira, S., Hamon, N., Bayle, P.A., Mouret, S., Clery-Barraud, C., Boudry, I., Douki, T., 2015. A guanine-ethylthioethyl-glutathione adduct as a major DNA lesion in the skin and in organs of mice exposed to sulfur mustard. Toxicol. Lett. 233, 1–7.

Brookes, P., Lawley, P.D., 1960. The reaction of mustard gas with nucleic acids in vitro and in vivo. Biochem. J. 77, 478–484.

Brookes, P., Lawley, P.D., 1961. The reaction of mono- and di-functional alkylating agents with nucleic acids. Biochem. J. 80, 496–503.

Brookes, P., Lawley, P.D., 1963. Effects of alkylating agents on T2 and T4 bacteriophages. Biochem. J. 89, 138–144.

Calvo, J.A., Meira, L.B., Lee, C.Y., Moroski-Erkul, C.A., Abolhassani, N., Taghizadeh, K., Eichinger, L.W., Muthupalani, S., Nordstrand, L.M., Klungland, A., Samson, L.D., 2012. DNA repair is indispensable for survival after acute inflammation. J. Clin. Invest. 122, 2680–2689.

Candeias, S., Pons, B., Viau, M., Caillat, S., Sauvaigo, S., 2010. Direct inhibition of excision/synthesis DNA repair activities by cadmium: analysis on dedicated biochips. Mutat. Res. 694, 53–59.

Cappelli, E., Hazra, T., Hill, J.W., Slupphaug, G., Bogliolo, M., Frosina, G., 2001. Rates of base excision repair are not solely dependent on levels of initiating enzymes. Carcinogenesis 22, 387–393.

Chilcott, R.P., Jenner, J., Carrick, W., Hotchkiss, S.A.M., Rice, P., 2000. Human skin absorption of bis-2-(chloroethyl) sulphide (sulphur mustard) in vitro. J. Appl. Toxicol. 20, 349–355.

Cullumbine, H., 1946. The mode of penetration of the skin by mustard gas. Br. J. Dermatol. 58, 291–294.

de Rosa, V., Erkekoglu, P., Forestier, A., Favier, A., Hincal, F., Diamond, A.M., Douki, T., Rachidi, W., 2012. Low doses of selenium specifically stimulate the repair of oxidative DNA damage in LNCaP prostate cancer cells. Free Radic. Res. 46, 105–116.

Debiak, M., Kehe, K., Burkle, A., 2009. Role of poly(ADP-ribose) polymerase in sulfur mustard toxicity. Toxicology 263, 20–25.

Dorandeu, F., Taysse, L., Boudry, I., Foquin, A., Herodin, F., Mathieu, J., Daulon, S., Cruz, C., Lallement, G., 2011. Cutaneous challenge with chemical warfare agents in the SKH-1 hairless mouse. (I) Development of a model for screening studies in skin decontamination and protection. Hum. Exp. Toxicol. 30, 470–490.

Ebrahimkhani, M.R., Daneshmand, A., Mazumder, A., Allocca, M., Calvo, J.A., Abolhassani, N., Jhun, I., Muthupalani, S., Ayata, C., Samson, L.D., 2014. Aag-initiated base excision repair promotes ischemia reperfusion injury in liver, brain, and kidney. Proc. Natl. Acad. Sci. U. S. A. 111, E4878–E4886.

Engelward, B.P., Weeda, G., Wyatt, M.D., Broekhof, J.L., de Wit, J., Donker, I., Allan, J. M., Gold, B., Hoeijmakers, J.H., Samson, L.D., 1997. Base excision repair deficient mice lacking the Aag alkyladenine DNA glycosylase. Proc. Natl. Acad. Sci. U. S. A. 94, 13087–13092.

Fidder, A., Moes, G.W.H., Scheffer, A.G., Vanderschans, G.P., Baan, R.A., Dejong, L.P.A., Benschop, H.P., 1994. Synthesis, characterization and quantitation of the major adducts formed between sulfur mustard and DNA of calf thymus and human blood. Chem. Res. Toxicol. 7, 199–204.

Forestier, A., Douki, T., Sauvaigo, S., Rosa, V.D., Demeilliers, C., Rachidi, W., 2012. Alzheimer's disease-associated neurotoxic Peptide amyloid-beta impairs base excision repair in human neuroblastoma cells. Int. J. Mol. Sci. 13, 14766–14787.

Garreau-Balandier, I., Lefebvre, M., Jacquard, S., Caillat, S., Cruz-Rodriguez, L., Ishak, L., Agier, V., Morel, F., Lachaume, P., Dubessay, P., Sauvaigo, S., Alziari, S., Vernet, P., 2014. A comprehensive approach to determining BER capacities and their change with aging in *Drosophila* melanogaster mitochondria by oligonucleotide microarray. FEBS Lett. 588, 1673–1679.

Ghanei, M., Poursaleh, Z., Harandi, A.A., Emadi, S.E., Emadi, S.N., 2010. Acute and chronic effects of sulfur mustard on the skin: a comprehensive review. Cutan. Ocul. Toxicol. 29, 269–277.

Glebova, K., Veiko, N., Kostyuk, S., Izhevskaya, V., Baranova, A., 2015. Oxidized extracellular DNA as a stress signal that may modify response to anticancer therapy. Cancer Lett. 356, 22–33.

Goswami, D.G., Kumar, D., Tewari-Singh, N., Orlicky, D.J., Jain, A.K., Kant, R., Rancourt, R.C., Dhar, D., Inturi, S., Agarwal, C., White, C.W., Agarwal, R., 2015. Topical nitrogen mustard exposure causes systemic toxic effects in mice. Exp. Toxicol. Pathol. 67, 161–170.

Hoeijmakers, J.H.J., 2001. Genome maintenance mechanisms for preventing cancer. Nature 411, 366–374.

Jowsey, P.A., Williams, F.M., Blain, P.G., 2012. DNA damage responses in cells exposed to sulphur mustard. Toxicol. Lett. 209, 1–10.

Kehe, K., Balszuweit, F., Steinritz, D., Thiermann, H., 2009. Molecular toxicology of sulfur mustard-induced cutaneous inflammation and blistering. Toxicology 263, 12–19.

Kircher, M., Fleer, R., Ruhland, A., Brendel, M., 1979. Biological and chemical effects of mustard gas in yeast. Mutat. Res. 63, 273–289.

Lawley, P.D., Brookes, P., 1965. Molecular mechanism of the cytotoxic action of difunctional alkylating agents and of resistance to this action. Nature 206, 480–483.

Liu, D., Pan, L., Yang, H., Wang, J., 2014. A physiologically based toxicokinetic and toxicodynamic model links the tissue distribution of benzo[a]pyrene and toxic effects in the scallop *Chlamys farreri*. Environ. Toxicol. Pharmacol. 37, 493–504.

Ludlum, D.B., Austinritchie, P., Hagopian, M., Niu, T.Q., Yu, D., 1994. Detection of sulfur mustard-induced DNA modifications. Chem. Biol. Interact. 91, 39–49.

Luncsford, P.J., Manvilla, B.A., Patterson, D.N., Malik, S.S., Jin, J., Hwang, B.J., Gunther, R., Kalvakolanu, S., Lipinski, L.J., Yuan, W., Lu, W., Drohat, A.C., Lu, A.L., Toth, E.A., 2013. Coordination of MYH DNA glycosylase and APE1 endonuclease activities via physical interactions. DNA Repair 12, 1043–1052.

Marie, C., Bouchard, M., Heredia-Ortiz, R., Viau, C., Maitre, A., 2010. A toxicokinetic study to elucidate 3-hydroxybenzo(a) pyrene atypical urinary excretion profile following intravenous injection of benzo(a) pyrene in rats. J. Appl. Toxicol. 30, 402–410.

Martin, O.A., Redon, C.E., Nakamura, A.J., Dickey, J.S., Georgakilas, A.G., Bonner, W.M., 2011. Systemic DNA damage related to cancer. Cancer Res. 71, 3437–3441.

Matijasevic, Z., Precopio, M.L., Snyder, J.E., Ludlum, D.B., 2001. Repair of sulfur mustard-induced DNA damage in mammalian cells measured by a host cell reactivation assay. Carcinogenesis 22, 661–664.

Matijasevic, Z., Stering, A., Niu, T.Q., Austin-Ritchie, P., Ludlum, D.B., 1996. Release of sulfur mustard-modified DNA bases by *Escherichia coli* 3-methyladenine DNA glycosylase II. Carcinogenesis 17, 2249–2252.

Matijasevic, Z., Volkert, M.R., 2007. Base excision repair sensitizes cells to sulfur mustard and chloroethyl ethyl sulfide. DNA Repair 6, 733–741.

Millau, J.F., Raffin, A.L., Caillat, S., Claudet, C., Arras, G., Ugolin, N., Douki, T., Ravanat, J. L., Breton, J., Oddos, T., Dumontet, C., Sarasin, A., Chevillard, S., Favier, A., Sauvaigo, S., 2008. A microarray to measure repair of damaged plasmids by cell lysates. Lab Chip 8, 1713–1722.

Momeni, A.Z., Enshaeih, S., Meghdadi, M., Amindjavaheri, M., 1992. Skin manifestations of mustard gas. A clinical study of 535 patients exposed to mustard gas. Arch. Dermatol. 128, 775–780.

Mouret, S., Wartelle, J., Batal, M., Emorine, S., Bertoni, M., Poyot, T., Cléry-Barraud, C., El Bakdouri, N., Peinnequin, A., Douki, T., Boudry, I., 2015. Time course of skin features and inflammatory biomarkers after liquid sulfur mustard exposure in SKH-1 hairless mice. Toxicol. Lett. 232, 68–78.

Oksenych, V., Bernardes de Jesus, B., Zhovmer, A., Egly, J.M., Coin, F., 2009. Molecular insights into the recruitment of TFIIH to sites of DNA damage. EMBO J. 28, 2971–2980.

Pal, A., Tewari-Singh, N., Gu, M., Agarwal, C., Huang, J., Day, B.J., White, C.W., Agarwal, R., 2009. Sulfur mustard analog induces oxidative stress and activates signaling cascades in the skin of SKH-1 hairless mice. Free Radic. Biol. Med. 47, 1640–1651.

Papirmeister, B., Gross, C.L., Meier, H.L., Petrali, J.P., Johnson, J.B., 1985. Molecular basis for mustard-induced vesication. Fundam. Appl. Toxicol. 5, 134–149.

Pons, B., Belmont, A.S., Masson-Genteuil, G., Chapuis, V., Oddos, T., Sauvaigo, S., 2010. Age-associated modifications of Base Excision Repair activities in human skin fibroblast extracts. Mech. Ageing Dev. 131, 661–665.

Robertson, A.B., Klungland, A., Rognes, T., Leiros, I., 2009. DNA repair in mammalian cells. Cell Mol. Life Sci. 66, 981–993.

Smith, K.J., Hurst, C.G., Moeller, R.B., Skelton, H.G., Sidell, F.R., 1995. Sulfur mustard: its continuing threat as a chemical warfare agent, the cutaneous lesions induced, progress in understanding its mechanism of action, its long-term health effects, and new developments for protection and therapy. J. Am. Acad. Dermatol. 32, 765–776.

Smith, S.A., Engelward, B.P., 2000. In vivo repair of methylation damage in Aag 3-methyladenine DNA glycosylase null mouse cells. Nucl. Acids Res. 28, 3294–3300.

Tewari-Singh, N., Jain, A.K., Inturi, S., Agarwal, C., White, C.W., Agarwal, R., 2012. Silibinin attenuates sulfur mustard analog-induced skin injury by targeting multiple pathways connecting oxidative stress and inflammation. PLoS One 7, 1–12.

van der Schans, G.P., Mars-Groenendijk, R., de Jong, L.P.A., Benschop, H.P., Noort, D., 2004. Standard operating procedure for immunuslotblot assay for analysis of DNA/sulfur mustard adducts in human blood and skin. J. Anal. Toxicol. 28, 316–319.

Visnes, T., Akbari, M., Hagen, L., Slupphaug, G., Krokan, H.E., 2008. The rate of base excision repair of uracil is controlled by the initiating glycosylase. DNA Repair 7, 1869–1881.

Wattana, M., Bey, T., 2009. Mustard gas or sulfur mustard: an old chemical agent as a new terrorist threat. Prehosp. Disaster Med. 24, 19–29.

Yue, L., Wei, Y., Chen, J., Shi, H., Liu, Q., Zhang, Y., He, J., Guo, L., Zhang, T., Xie, J., Peng, S., 2014. Abundance of four sulfur mustard-DNA adducts ex vivo and in vivo revealed by simultaneous quantification in stable isotope dilution-ultrahigh performance liquid chromatography-tandem mass spectrometry. Chem. Res. Toxicol. 27, 490–500.

Yue, L., Zhang, Y., Chen, J., Zhao, Z., Liu, Q., Wu, R., Guo, L., He, J., Zhao, J., Xie, J., Peng, S., 2015. Distribution of DNA adducts and corresponding tissue damage of sprague-dawley rats with percutaneous exposure to sulfur mustard. Chem. Res. Toxicol. 28, 532–540.